

Homework 3 (Tasks 1-19) in EL2450 Hybrid and Embedded Control Systems

Rene Garcia	Daniel Skott	Joel Aggefors
20010124-5512	20020314-5214	20030301-4575
reneogt@kth.se	dskott@kth.se	joelag@kth.se

Jenis Jain	David Ring
20030424-T490	20000111-2374
jjjain@kth.se	dring@kth.se

March 1, 2026

Task 1: Compute u_r and u_l from (v, ω)

The robot inputs are defined as:

$$v = \frac{u_r + u_l}{2}, \quad \omega = u_r - u_l. \quad (1)$$

From (1), multiply the first equation by 2:

$$2v = u_r + u_l. \quad (2)$$

Now add (2) and the second equation in (1):

$$2v + \omega = (u_r + u_l) + (u_r - u_l) = 2u_r \Rightarrow u_r = v + \frac{\omega}{2}. \quad (3)$$

Similarly, subtract the second equation in (1) from (2):

$$2v - \omega = (u_r + u_l) - (u_r - u_l) = 2u_l \Rightarrow u_l = v - \frac{\omega}{2}. \quad (4)$$

Therefore, the wheel speeds corresponding to (v, ω) are:

$$u_r = v + \frac{\omega}{2}, \quad u_l = v - \frac{\omega}{2}$$

(5)

Task 2

(a) Discretization, numbering , and atomic propositions

Workspace: $[-1.5, 1.5] \times [-1.5, 1.5]$ (meters). A discretization with $K = 36$ gives a 6×6 grid.

R_6 G,S	R_7 B	R_{18} -	R_{19} O	R_{30} -	R_{31} R,G,O
R_5 -	R_8 R,O	R_{17} -	R_{20} R	R_{29} B,O	R_{32} R
R_4 -	R_9 G	R_{16} -	R_{21} B	R_{28} -	R_{33} -
R_3 O	R_{10} O	R_{15} -	R_{22} O	R_{27} -	R_{34} -
R_2 G	R_{11} R,O	R_{14} -	R_{23} B	R_{26} R,O	R_{35} -
R_1 R	R_{12} -	R_{13} -	R_{24} -	R_{25} G	R_{36} B

Figure 1: Workspace discretization with $K = 36$ regions. Labels indicate where atomic propositions hold.

The regions are numbered in a *column-wise snake* pattern: start at the bottom-left with R_1 , go *up* in the first column, then *down* in the next column, and so on. Thus, the 6×6 numbering is:

R_6	R_7	R_{18}	R_{19}	R_{30}	R_{31}
R_5	R_8	R_{17}	R_{20}	R_{29}	R_{32}
R_4	R_9	R_{16}	R_{21}	R_{28}	R_{33}
R_3	R_{10}	R_{15}	R_{22}	R_{27}	R_{34}
R_2	R_{11}	R_{14}	R_{23}	R_{26}	R_{35}
R_1	R_{12}	R_{13}	R_{24}	R_{25}	R_{36}

Atomic propositions: Let $AP = \{\text{red}, \text{blue}, \text{green}, \text{obstacle}\}$. The propositions are specified by the following positions (meters):

- **obstacle** centers (spheres of radius 0.05 m) at:

$$(-0.75, 0.75), (0.25, 1.25), (0.75, 0.75), (0.25, -0.25), (0.75, -0.75), (-0.75, -0.75), \\ (-0.75, -0.25), (1.25, 1.25), (-1.25, -0.25).$$

- **red** holds at:

$$(-0.75, 0.7), (0.2, 0.7), (1.25, 1.25), (1.2, 0.8), (0.8, -0.8), (-0.9, -0.8), (-1.25, -1.25).$$

- **blue** holds at:

$$(-0.75, 1.4), (0.9, 0.9), (0.3, 0.2), (0.25, -0.75), (1.2, -1.4).$$

- **green** holds at:

$$(-1.23, 1.25), (1.25, 1.25), (-0.9, 0.2), (-1.2, -0.7), (0.6, -1.2).$$

Labeling rule: a proposition is true in the region that contains its given position, i.e.

$$p \in L(R_i) \iff (x_p, y_p) \in R_i, \quad p \in AP.$$

The start position is $(-1.25, 1.25)$, hence $S_0 = \{R_6\}$.

(b) Cell size dx, dy

Since the side length is 3 m and there are 6 cells per side,

$$dx = \frac{3}{6} = 0.5 \text{ m}, \quad dy = \frac{3}{6} = 0.5 \text{ m}.$$

(c) Comment on the choice $K = 36$

A 6×6 grid provides a finer abstraction than coarse grids (better separation of obstacles/colored areas), but increases the number of states and transitions compared to smaller K .

(d) Transition system $T = (S, S_0, \Sigma, \rightarrow, AP, L)$

$$S = \{R_1, \dots, R_{36}\}, \quad S_0 = \{R_6\}, \quad \Sigma = \{\text{Up, Down, Left, Right}\}, AP = \{\text{red, blue, green, obstacle}\}.$$

The transition relation \rightarrow is the 4-neighborhood relation on the grid:

$$R_i \xrightarrow{\sigma} R_j \iff R_j \text{ is the adjacent region to } R_i \text{ in direction } \sigma \in \Sigma.$$

The labeling function $L : S \rightarrow 2^{AP}$ is defined using the point-in-region rule above.

Task 3: Find an infinite path satisfying the specification

Specification: (i) visit **red** infinitely often, (ii) whenever the robot is in a **red** region, the *next* region is **blue**, (iii) never enter a region labeled **obstacle**.

Chosen red–blue pair: From the labeling in Task 2, $R_{20} \in \text{red}$ and $R_{21} \in \text{blue}$, and they are adjacent in the 6×6 grid (R_{21} is directly below R_{20}). Moreover, $R_{20}, R_{21} \notin \text{obstacle}$.

A valid infinite path: Starting from $S_0 = \{R_6\}$, one feasible prefix to reach R_{20} without entering obstacles is

$$R_6 \rightarrow R_7 \rightarrow R_{18} \rightarrow R_{17} \rightarrow R_{16} \rightarrow R_{21} \rightarrow R_{20}.$$

Then, repeat the 2-cycle (R_{20}, R_{21}) forever:

$$\pi = \underbrace{(R_6, R_7, R_{18}, R_{17}, R_{16}, R_{21}, R_{20})}_{\text{prefix}} \cdot \underbrace{(R_{21}, R_{20})^\omega}_{\text{suffix repeated forever}}.$$

Why π satisfies the specification:

- π visits R_{20} infinitely often, and $R_{20} \in \text{red}$, hence **red** is visited infinitely often.
- Every time π is in R_{20} (a **red** region), the next state is R_{21} and $R_{21} \in \text{blue}$, so the “after **red** next is **blue**” condition holds.
- All regions used in π are chosen outside the set of **obstacle** regions, hence obstacles are never entered.

Task 4

The hybrid strategy prevents entering unintended regions by separating the motion into two simple phases. First, the robot uses a rotation mode with (approximately) zero forward speed, i.e., $v \approx 0$, so it turns in place to align its heading with the straight line connecting the center of the current region to the center of the target (neighbor) region. Because the robot does not translate during this phase, it stays close to the current region center and does not drift into adjacent regions. Second, the robot switches to a line-following mode and drives forward while tracking that same center-to-center line. For neighboring regions, this line segment lies within the union of the two adjacent cells. Therefore, if the tracking error is kept small, the robot remains inside only the current and target regions during the transition, and it avoids passing through any other region that could contain an obstacle.

Task 5

During the rotation mode, the controller is

$$\omega[k] = K_{\Psi,1}(\theta_R - \theta[k]). \quad (6)$$

The robot yaw dynamics satisfy

$$\dot{\theta}(t) = \frac{R}{L}\omega(t). \quad (7)$$

Using forward Euler discretization with sampling time h ,

$$\theta[k+1] = \theta[k] + h \frac{R}{L} \omega[k]. \quad (8)$$

Substituting (6) into (8) and defining the error $e[k] = \theta_R - \theta[k]$, we obtain

$$e[k+1] = \left(1 - \frac{hR}{L}K_{\Psi,1}\right)e[k]. \quad (9)$$

For asymptotic stability of the discrete-time error dynamics, we require

$$\left|1 - \frac{hR}{L}K_{\Psi,1}\right| < 1 \iff 0 < \frac{hR}{L}K_{\Psi,1} < 2 \iff \boxed{0 < K_{\Psi,1} < \frac{2L}{hR}}. \quad (10)$$

A practical choice is to pick $K_{\Psi,1}$ well inside this interval (e.g., $K_{\Psi,1} = \alpha \frac{L}{hR}$ with $\alpha \in (0, 1)$) to avoid oscillations and actuator saturation.

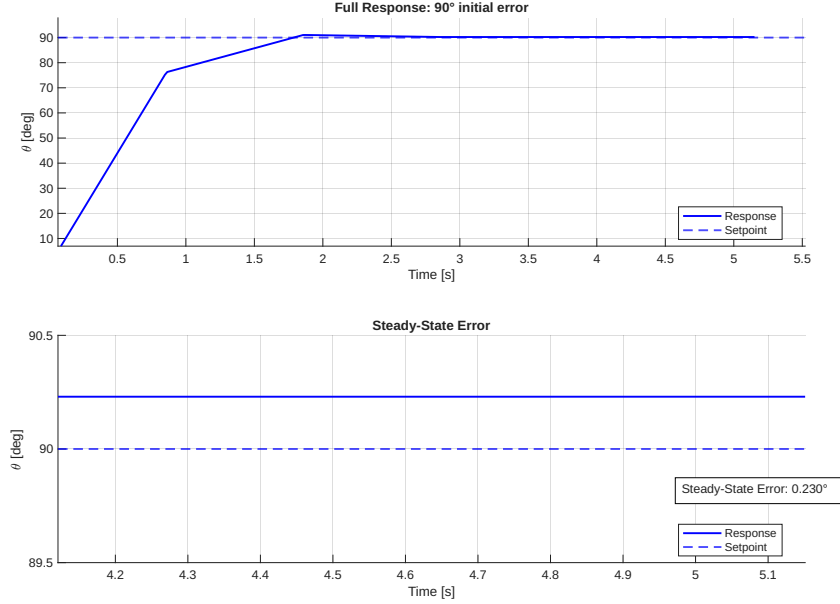
Task 6

First we define the proportional constant value. Given eq. (10), we could aim for a deadbeat controller by setting $K_{\Psi,1} = \frac{2L}{hR}$, nonetheless, this would force the controller to correct the error in one sampling step, completely ignoring physical limits and inertia. A safer value to chose is the middle of the stability range:

$$K_{\Psi,1} = \frac{1}{2} \frac{2L}{hR} = \frac{L}{hR} = \frac{0.16}{0.033 * 1} = 4.85 \quad [1/s]. \quad (11)$$

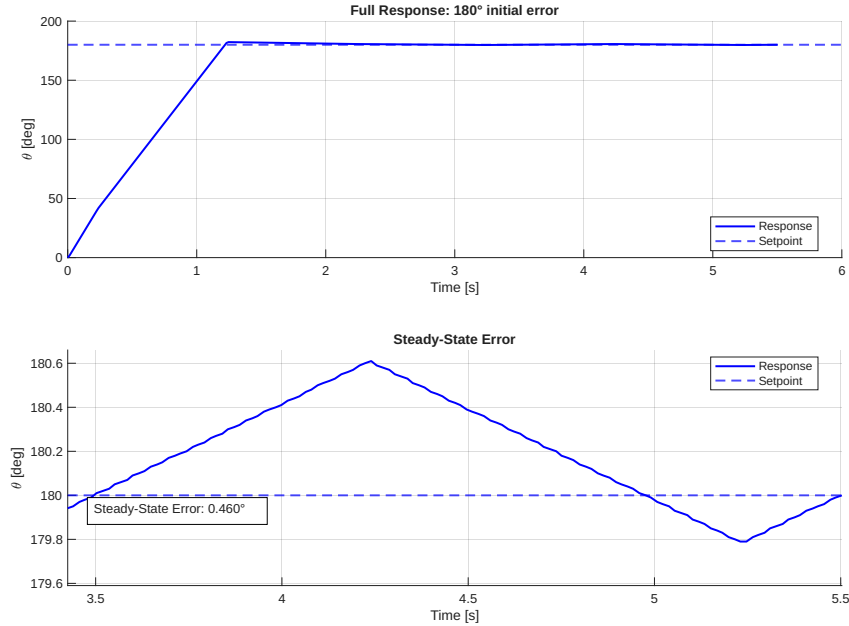
To test the performance of the controller, we run 2 different scenarios:

- Scenario 1: $\theta_R = 90^\circ$, $\theta[0] = 0^\circ$ (90 degree turn)



For this case, the wheels stop turning at around 1.85 s , and there is a **steady-state** error of 0.23° .

- Scenario 2: $\theta_R = 180^\circ$, $\theta[0] = 0^\circ$ (180 degree turn)



For this case, there is a constant ripple that slowly rotates the robot back and forth around the target angle. This is a case of limit cycle caused by quantization. For this case, we consider the largest error, that is, the peak of the ripple. Then, the **steady-state** error is 0.46° .

In general, can see that the controller **asymptotically stabilizes** the error in both scenarios, as we don't see divergence over time.

Task 7

Assume $\theta[k+1] = \theta[k] = \theta$ so $v_c = [\cos \theta \ \sin \theta]^\top$ is constant and $v_c^\top v_c = 1$. Using $\dot{p} = Rvv_c$ with $p = [x \ y]^\top$ and forward Euler,

$$p[k+1] = p[k] + hRv[k]v_c \Rightarrow \Delta_0[k+1] = \Delta_0[k] - hRv[k]v_c.$$

Premultiplying by v_c^\top yields

$$d_0[k+1] = v_c^\top \Delta_0[k+1] = d_0[k] - hRv[k].$$

With $v[k] = K_{\omega,1}d_0[k]$,

$$d_0[k+1] = (1 - hRK_{\omega,1})d_0[k].$$

Asymptotic stability requires $|1 - hRK_{\omega,1}| < 1$, hence

$$0 < K_{\omega,1} < \frac{2}{hR}.$$

Task 8

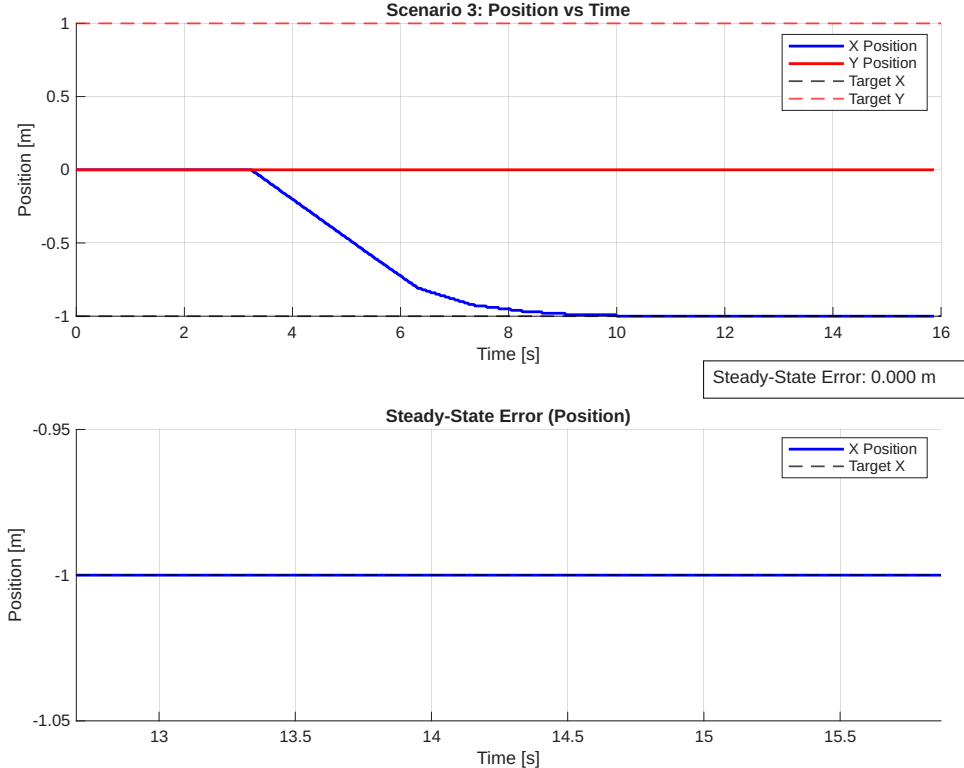
Similarly to Task 6, we select $K_{\omega,1}$ in the middle of the stability interval:

$$K_{\omega,1} = \frac{1}{2} \frac{2}{hR} = \frac{1}{hR} = \frac{1}{0.033 * 1} = 30.3 \quad [\frac{1}{m \cdot s}]. \quad (12)$$

To test the performance of the controller, we run 1 single scenario:

- **Scenario 1: Diagonal Error**

Starting position: $(x_0, y_0) = (0, 0)$, $\theta = 0^\circ$ Target: $(x_g, y_g) = (-1, 1)$

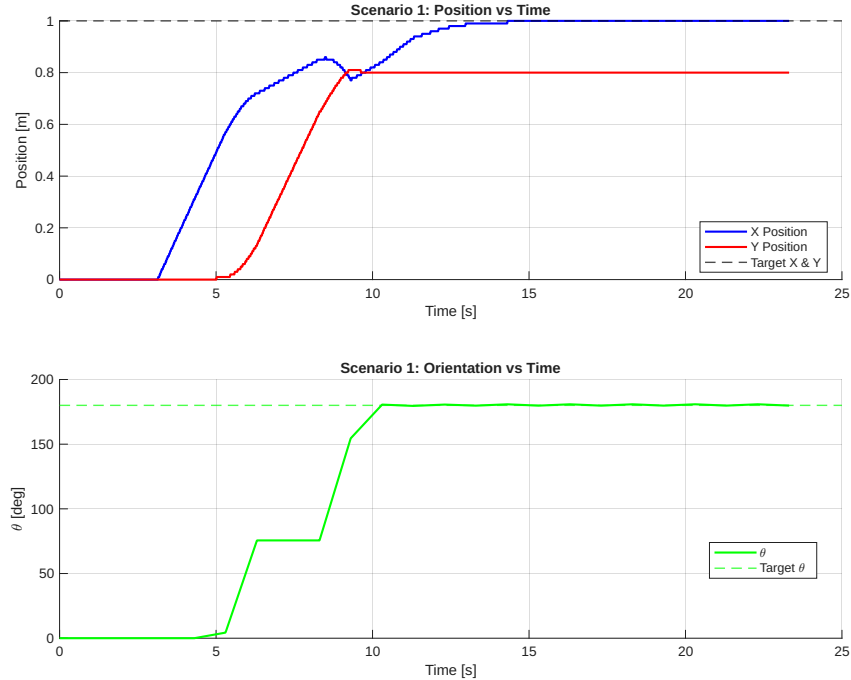


As we can see, the robot moves only in the x direction, as this is the direction it is facing initially. The controller successfully reduces the X error to zero, but the Y error remains.

Task 9

To test both controllers together, we simulate an scenario where we have error in the position and angle, and enable both controllers.

- **Scenario 1:** Starting position: $(x_0, y_0) = (0, 0)$, $\theta = 0^\circ$ Target: $(x_g, y_g) = (1, 1)$, $\theta^R = 180^\circ$



As we can see, the angle error is corrected first, and then blocking the possibility of correcting the position error. This can become a race condition.

Task 10

Assume $\theta[k] = \theta_g$, hence $v_g = [\cos \theta_g \quad \sin \theta_g]^\top$ is constant and $v_g^\top v_g = 1$. With $\dot{p} = Rvv_g$ and forward Euler,

$$p[k+1] = p[k] + hR v[k] v_g \Rightarrow \Delta_g[k+1] = \Delta_g[k] - hR v[k] v_g.$$

Premultiplying by v_g^\top yields

$$d_g[k+1] = v_g^\top \Delta_g[k+1] = d_g[k] - hR v[k].$$

Using $v[k] = K_{\omega,2} d_g[k]$,

$$d_g[k+1] = (1 - hRK_{\omega,2}) d_g[k].$$

Asymptotic stability requires $|1 - hRK_{\omega,2}| < 1$, hence

$$\boxed{0 < K_{\omega,2} < \frac{2}{hR}}.$$

A practical choice is to select $K_{\omega,2}$ well inside this interval (e.g., $K_{\omega,2} = \alpha \frac{1}{hR}$ with $\alpha \in (0, 1)$) to ensure monotone convergence and robustness to discretization/actuator limits.

Task 11

The closed-loop dynamics of d_g are

$$d_g[k+1] = (1 - HRK_{\omega,2})d_g[k].$$

For $0 < HRK_{\omega,2} < 2$, we have $|1 - HRK_{\omega,2}| < 1$, hence

$$\lim_{k \rightarrow \infty} d_g[k] = 0.$$

Thus, d_g is asymptotically stabilized in 0.

However, since $\omega[k] = 0$, the orientation θ remains constant and the robot moves along a fixed straight line. If the initial orientation is not aligned with the goal direction, the robot cannot correct lateral error. Therefore,

$$[x[k], y[k]]^T \not\rightarrow [x_g, y_g]^T$$

for arbitrary initial orientations.

In Fig. 2 we can see that the robot travels in a straight line and that it comes closer to the goal. Another observation not observable in the graph is that the robot slows down and stops at the goal.

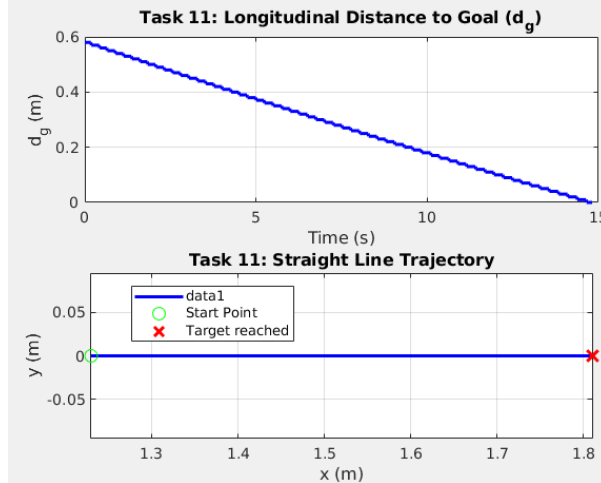


Figure 2: Result from discrete straight line controller

Task 12

The controller for line-following (part II) is

$$\omega[k] = K_{\Psi,2} d_p[k].$$

Assume the robot is on the line from (x_0, y_0) to (x_g, y_g) and θ is close to θ_g so that

$$d_p[k] \approx p(\theta_g - \theta[k]), \quad p > 0.$$

Let $e[k] = \theta_g - \theta[k]$, hence $d_p[k] \approx p e[k]$. From the yaw dynamics $\dot{\theta} = \frac{R}{L}\omega$ and forward Euler with sampling time h ,

$$\theta[k+1] = \theta[k] + h \frac{R}{L} \omega[k].$$

Therefore,

$$e[k+1] = \theta_g - \theta[k+1] = e[k] - h \frac{R}{L} \omega[k] = e[k] - h \frac{R}{L} K_{\Psi,2} d_p[k] \approx \left(1 - h \frac{R}{L} K_{\Psi,2} p\right) e[k].$$

Multiplying by p gives the discrete-time dynamics of d_p :

$$d_p[k+1] \approx \left(1 - h \frac{R}{L} K_{\Psi,2} p\right) d_p[k].$$

Thus $d_p[k]$ is asymptotically stabilized in 0 iff

$$\left|1 - h \frac{R}{L} K_{\Psi,2} p\right| < 1 \iff \boxed{0 < K_{\Psi,2} < \frac{2L}{hRp}}.$$

Choice of $K_{\Psi,2}$. Select $K_{\Psi,2}$ strictly inside the stability interval, e.g.

$$K_{\Psi,2} = \alpha \frac{L}{hRp}, \quad \alpha \in (0, 1),$$

which yields the contraction factor $1 - \alpha$ (monotone convergence) and keeps the closed-loop behavior consistent when the sampling time h changes.

Task 13

If we model the corrective input using the (nonlinear) sine term, for instance

$$d_p \approx p \sin(\theta_g - \theta),$$

then p plays the role of a proportional gain. Increasing p improves the tracking accuracy of θ to the goal θ_g . However, if p is chosen too large the closed-loop trajectory typically oscillates around θ_g and cannot settle at a point. Intuitively this happens because the region of attraction (the set of initial conditions that converge to θ_g) shrinks as p increases, so overly large gains reduce stability margins and promote sustained oscillations.

The angular controller

$$\omega[k] = K_{\Psi,2} d_p[k] \tag{13}$$

was implemented using the exact nonlinear definition of d_p from (13), while the translational velocity was set to $v = 0$ to isolate the rotational dynamics.

The lateral deviation is defined as

$$d_p[k] = v_{g,\perp}^T v_p[k],$$

where

$$v_p[k] = \begin{bmatrix} x[k] + p \cos \theta[k] - x_0 \\ y[k] + p \sin \theta[k] - y_0 \end{bmatrix}.$$

Simulation results show that the robot rotates in place and $d_p[k]$ converges asymptotically to zero without steady-state error. The decay is approximately exponential, consistent with the discrete-time dynamics derived in Task 12:

$$d_p[k+1] = \left(1 - \frac{hR}{L} K_{\Psi,2} p\right) d_p[k].$$

For

$$K_{\Psi,2} = \frac{\alpha L}{hRp}, \quad 0 < \alpha < 1,$$

the closed-loop pole becomes $1-\alpha$, which lies inside the unit circle. Hence, the equilibrium $d_p = 0$ is asymptotically stable.

The simulation confirms the theoretical stability analysis.

In fig 3 we can see that the angle slowly goes from 0 degrees to 90 degrees when the goal point changes. in this simulation the new goal was 90 degrees above the robot with means that it reached the goal in the simulation.

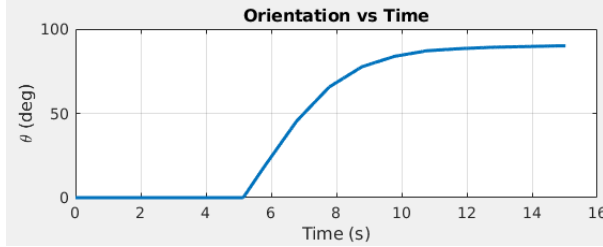


Figure 3: theta over time task 13

Remark. In particular one must not replace $\sin(\theta_g - \theta)$ by $\theta_g - \theta$ unless the small-angle approximation is explicitly justified.

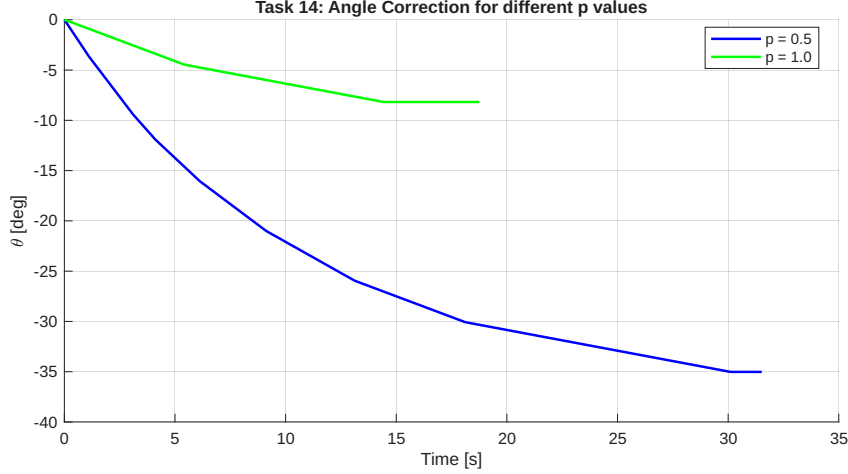
Task 14

From Task 12, the stability condition for the line-following controller is

$$0 < K_{\Psi,2} < \frac{2L}{hRp}.$$

Since p appears in the denominator, a larger p shrinks the stability interval and reduces the maximum admissible gain $K_{\Psi,2}$. We compare two values experimentally:

- $p = 0.5$: stability bound $K_{\Psi,2} < \frac{2 \cdot 0.16}{1 \cdot 0.033 \cdot 0.5} \approx 19.4$. The wide stability margin allows a strong corrective input without oscillations. The measured displacement error is $y_{\text{err}} = 0.1$ m.
- $p = 1.0$: stability bound $K_{\Psi,2} < \frac{2 \cdot 0.16}{1 \cdot 0.033 \cdot 2} \approx 4.85$. The narrow margin means the same gain C pushes the system closer to the stability boundary, resulting in slower or oscillatory convergence. The measured displacement error is $y_{\text{err}} = 0.5$ m.



As can be seen in the plot, $p = 0.5$ provides a smoother and faster convergence to the target angle $\theta_g = 90^\circ$, while $p = 1.0$ leads to a noticeably slower response with a larger displacement error. Therefore, we choose $p = 0.5$ because it offers a wider stability margin, better transient behavior, and a significantly smaller steady-state displacement error.

Task 15

When both controllers are enabled, the longitudinal error d_g and the lateral error d_p converge simultaneously to zero. In contrast, when only the translational controller is active, d_g decreases while d_p remains nonzero. When only the angular controller is enabled, d_p converges but no progress toward the goal is achieved. The combined controller therefore achieves stable line-following behaviour.

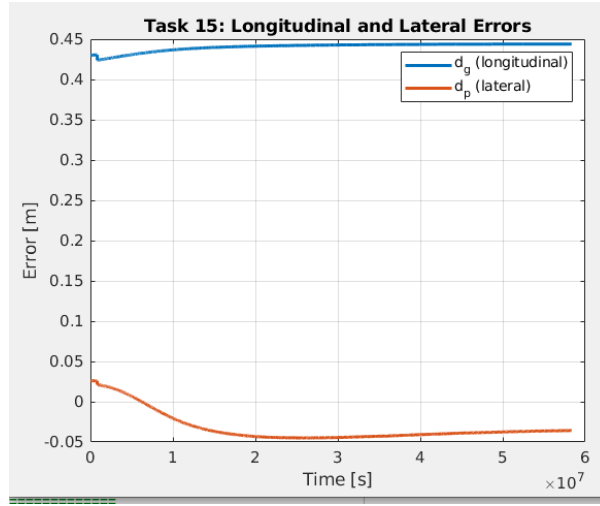


Figure 4:

Task 16 : Hybrid automaton

Define the hybrid automaton $H = (Q, X, Init, f, D, E, G, R)$.

Discrete states.

$$Q = \{q_{\text{rot}}, q_{\text{line}}\},$$

where q_{rot} aligns the robot with the goal direction and q_{line} performs line-following / go-to-goal.

Continuous state and initialization.

$$X = \begin{bmatrix} x \\ y \\ \theta \end{bmatrix}, \quad Init = \left\{ (q_{\text{rot}}, X) \mid X = \begin{bmatrix} x_s \\ y_s \\ \theta_s \end{bmatrix} \right\}.$$

Continuous dynamics (closed-loop). Robot kinematics:

$$\dot{x} = Rv \cos \theta, \quad \dot{y} = Rv \sin \theta, \quad \dot{\theta} = \frac{R}{L}\omega.$$

Let $\theta_R = \text{atan2}(y_g - y, x_g - x)$.

Mode q_{rot} :

$$\omega = K_{\Psi,1}(\theta_R - \theta), \quad v = K_{\omega,1}d_0.$$

Mode q_{line} :

$$v = K_{\omega,2}d_g, \quad \omega = K_{\Psi,2}d_p.$$

Domains.

$$D(q_{\text{rot}}) = D(q_{\text{line}}) = \mathbb{R}^2 \times (-180^\circ, 180^\circ].$$

Edges and guards.

$$E = \{(q_{\text{rot}}, q_{\text{line}}), (q_{\text{line}}, q_{\text{rot}})\}.$$

Using thresholds $\varepsilon_\theta > 0$ and $\varepsilon_g > 0$:

$$G(q_{\text{rot}}, q_{\text{line}}) = \{X : |\theta_R - \theta| \leq \varepsilon_\theta\}, \quad G(q_{\text{line}}, q_{\text{rot}}) = \{X : \|(x_g - x, y_g - y)\| \leq \varepsilon_g\}.$$

Resets. No state jump at switching (identity reset):

$$R(q_{\text{rot}}, q_{\text{line}}) : X^+ = X, \quad R(q_{\text{line}}, q_{\text{rot}}) : X^+ = X.$$

(If multiple waypoints are used, the next goal (x_g, y_g) is updated externally when ε_g is reached.)

Task 17

To implement the hybrid automaton we code conditions to make the robot firstly rotate (state q_{rot}) and then move forward in a line (state q_{line}). In Figure 5 is shown a simulation (continuous states) where node 5 is the start and node 4 is the goal, and in Figure 6 is shown the corresponding discrete states.

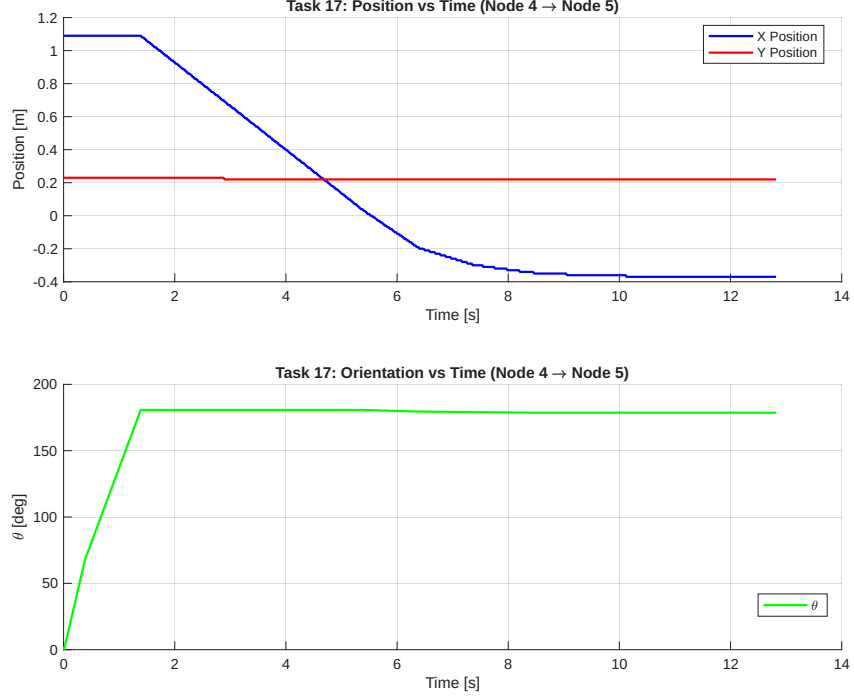


Figure 5: Plot of continuous states where robot starts at node 5 and given node 4 as goal.

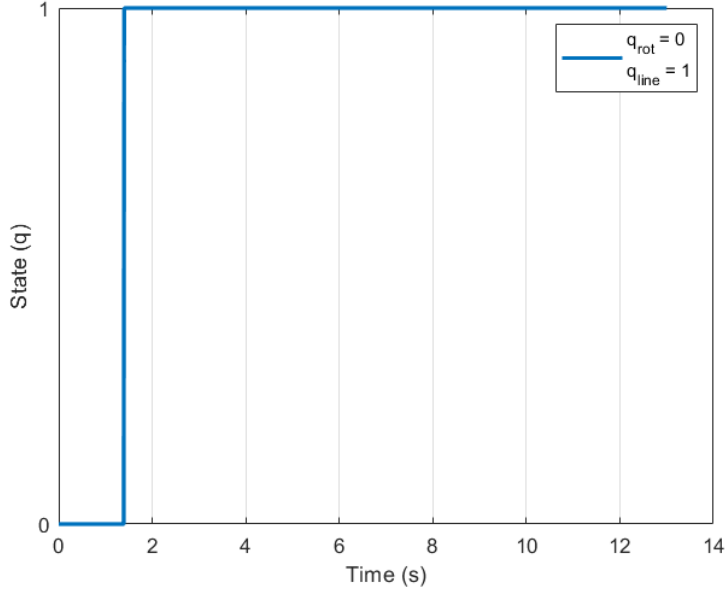


Figure 6: Plot of discrete states where robot starts at node 5 and given node 4 as goal.

Task 18

We execute the plan derived in Task 3 on the online simulator by programming the sequence of waypoints corresponding to the region centers along the path

$$R_6 \rightarrow R_7 \rightarrow R_{18} \rightarrow R_{17} \rightarrow R_{16} \rightarrow R_{21} \rightarrow R_{20} \rightarrow (R_{21}, R_{20})^\omega.$$

Each waypoint is the center (x_c, y_c) of the respective 0.5×0.5 m region. The hybrid automaton from Task 16 handles transitions between waypoints: the robot first rotates

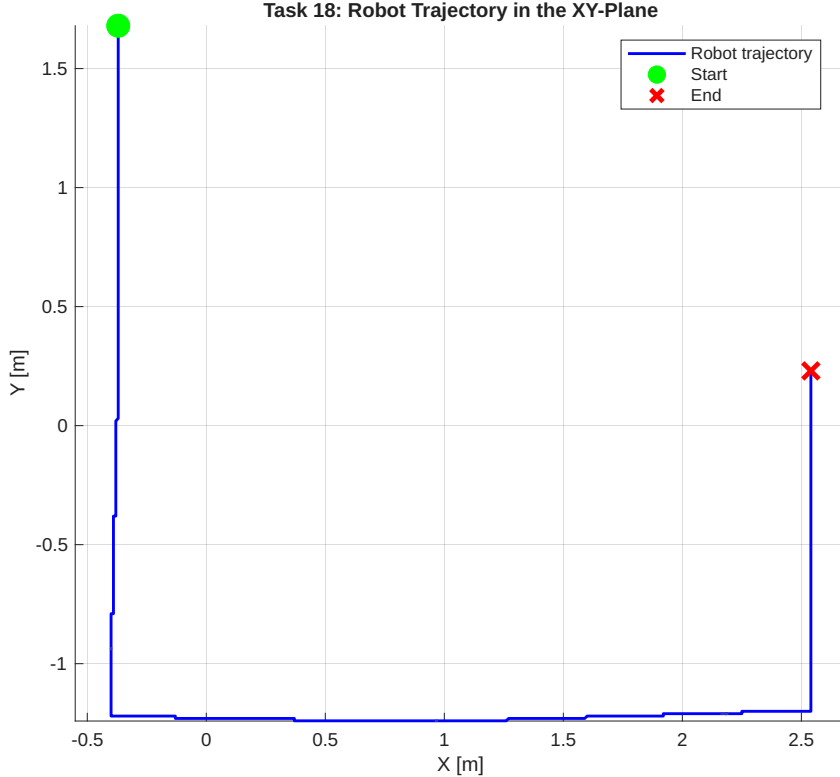


Figure 7: Trajectory of continuous state.

in place (q_{rot}) to align with the next waypoint, then drives in a straight line (q_{line}) while the line-following controller corrects lateral deviations.

Observations:

- The trajectory consists of clearly distinguishable straight-line segments connected by sharp turns at each waypoint, confirming that the rotate-then-drive strategy from Task 4 works as intended.
- The robot successfully follows the planned prefix path and reaches the $R_{20} \leftrightarrow R_{21}$ cycle, satisfying the specification (visit red infinitely often, always followed by blue, no obstacles entered).
- Small lateral offsets are visible along the straight segments due to the finite sampling time and the discrete nature of the controller, but these remain well within the 0.5 m cell width, so the robot does not enter unintended regions.
- At each waypoint the robot dwells briefly while rotating, which introduces a slight position drift. This is acceptable as long as the drift stays inside the current region.

Task 19: Safety Property Analysis

To safely transition between regions R_i and R_j , the robot must remain inside their union by minimizing drift. During rotation, slow convergence and residual forward velocity can push the robot beyond the 0.25 m safety limit. During line-following, the lookahead distance (p) dictates the lateral error (d_p). Safety therefore relies on fast rotation

convergence, tight switching thresholds (ε_θ and ε_g) to ensure proper alignment, and correctly tuned gains. Implementing $K_{\Psi,1}$, $K_{\Psi,2}$, and $p = 0.5$ successfully restricts lateral deviations below 0.25 m, according to the simulations.

References

- [1] Hassan K Khalil. *Nonlinear systems*. Prentice Hall, Upper Saddle river, 3. edition, 2002. ISBN 0-13-067389-7.
- [2] Tobias Oetiker, Hubert Partl, Irene Hyna, and Elisabeth Schlegl. *The Not So Short Introduction to L^AT_EX 2_&*. Oetiker, OETIKER+PARTNER AG, Aarweg 15, 4600 Olten, Switzerland, 2008. <http://www.ctan.org/info/lshort/>.
- [3] Shankar Sastry. *Nonlinear systems: analysis, stability, and control*, volume 10. Springer, New York, N.Y., 1999. ISBN 0-387-98513-1.